



Dalton
Transactions

**Photophysics and Reverse Saturable Absorption of Cationic
Dinuclear Iridium(III) Complexes Bearing Fluorenyl-
Tethered 2-(Quinolin-2-yl)quinoxaline Ligand**

Journal:	<i>Dalton Transactions</i>
Manuscript ID	DT-ART-06-2021-002176.R1
Article Type:	Paper
Date Submitted by the Author:	21-Aug-2021
Complete List of Authors:	Lu, Cuifen; North Dakota State University Lu, Taotao; North Dakota State University Cui, Peng; North Dakota State University, Department of Chemistry and Biochemistry Kilina, Svetlana; North Dakota State University, Chemistry and Biochemistry Sun, Wenfang; North Dakota State University, Chemistry

SCHOLARONE™
Manuscripts

ARTICLE

Photophysics and Reverse Saturable Absorption of Cationic Dinuclear Iridium(III) Complexes Bearing Fluorenyl-Tethered 2-(Quinolin-2-yl)quinoxaline Ligand

Received 00th January 20xx,
Accepted 00th January 20xx

DOI: 10.1039/x0xx00000x

Cuifen Lu,^{a,b,‡} Taotao Lu,^{a,‡} Peng Cui,^{c,a,d} Svetlana Kilina^a and Wenfang Sun^{a,*}

ABSTRACT: The synthesis, photophysics and reverse saturable absorption of two cationic dinuclear Ir(III) complexes bearing fluorenyl-tethered 2-(quinolin-2-yl)quinoxaline (quqo) ligand are reported in this paper. The two complexes possess intense and featureless diimine ligand localized ¹ILCT (intraligand charge transfer) / ¹π,π* absorption bands at ca. 330 and 430 nm, and weak ^{1,3}MLCT (metal-to-ligand charge transfer) / ^{1,3}LLCT (ligand-to-ligand charge transfer) absorption band at >500 nm. Both complexes exhibit weak dual phosphorescence at ca. 590 nm and 710 nm, which are attributed to the ³ILCT/³π,π* and ³MLCT/³LLCT states, respectively. The low-energy ³MLCT/³LLCT state also gives rise to moderately strong triplet excited-state absorption at 490–800 nm. Because of the stronger triplet excited-state absorption than the ground-state absorption of these complexes at 532 nm, both complexes manifest a moderate reverse saturable absorption (RSA) at 532 nm for ns laser pulses. Expansion of the π-conjugation of the fluorenyl-tethered diimine ligand in **Ir-1** causes a slight red-shift of the ¹ILCT/¹π,π* absorption bands in its UV-vis absorption spectrum and the ³MLCT/³LLCT absorption band in the transient absorption spectrum and slightly enhances the RSA at 532 nm compared to those of **Ir-2**. This work represents the first report on dinuclear Ir(III) complexes that exhibit RSA at 532 nm.

Introduction

Octahedral d⁶ Ir(III) complexes have attracted great interest among chemists and materials scientists during the past three decades because of their high triplet excited-state quantum yields, synthetic versatility, and excellent chemical and photo stabilities.^{1–4} The rich photophysical and electrochemical properties of these complexes prompt their potential applications in organic light-emitting devices (OLEDs),^{5–7} light-emitting electrochemical cells (LEECs),⁸ energy upconversion,⁹ nonlinear optics,^{10,11} photocatalysis,^{12,13} bioimaging and biosensing,¹⁴ and photodynamic therapy.^{15,16} Among the Ir(III) complexes, heteroleptic cationic Ir(III) complexes are more appealing because their ground- and excited-state properties can be readily tuned by structural modifications of the diimine (N[^]N) and/or cyclometalating (C[^]N) ligands.^{17–28}

There are two common strategies to tune the photophysical and electrochemical properties of Ir(III) complexes. One is to introduce different electron-donating or withdrawing substituents to the N[^]N and/or C[^]N ligands,^{17–19} which mainly adjusts the energy levels of the excited states without a significant impact on the nature of the excited states. The other strategy is to extend the π-conjugation of the N[^]N and/or C[^]N ligands,^{20–29} which can drastically alter the nature of the lowest triplet excited state. Bryce's group found that phosphorescence lifetime was increased when the π-conjugation of the N[^]N ligands was extended in cationic Ir(III) complexes.²¹ Huang's group revealed that the emission wavelength of the Ir(III) complexes was remarkably red-shifted by expanding the π-conjugation of the N[^]N ligand.²² Schanze's group²³ and our group^{10,26–29} discovered that the triplet excited-state lifetime was dramatically increased and the triplet excited-state absorption was enhanced by extending the π-conjugation of the N[^]N ligand *via* incorporation of π-conjugated substituents or benzannulation. Meanwhile, benzannulation on the N[^]N ligand at appropriate sites red-shifted the ground-state charge-transfer absorption band while keeping a reasonably long-lived triplet excited state.^{28,29}

While expanding the ligand π-conjugation in Ir(III) complexes has shown promising in improving the properties of the excited state, most of the reports were focused on the mononuclear Ir(III) complexes. Dinuclear Ir(III) complexes have been much underexplored due to (1) synthetic challenges and difficulty in separation of diastereomers or geometric isomers; (2) less predictable properties associated with complicated intra- and inter-

^a Department of Chemistry and Biochemistry, North Dakota State University, Fargo, ND 58108-6050, USA

^b Hubei Collaborative Innovation Center for Advanced Organometallic Materials & Ministry-of-Education Key Laboratory for the Synthesis and Application of Organic Functional Molecules, Hubei University, Wuhan, 430062, P. R. China

^c Key Laboratory of Eco-textiles, Ministry of Education, Jiangnan University, Wuxi, Jiangsu Province 214122, P. R. China

^d Materials and Nanotechnology Program, North Dakota State University, Fargo, ND 58108-6050, USA

‡ These two authors contributed equally to this project.

* Corresponding author. E-mail: Wenfang.Sun@ndsu.edu

Electronic Supplementary Information (ESI) available: ¹H NMR spectra, comparison of the experimental and calculated absorption spectra, solvent-dependent absorption and emission spectra, time-resolved transient absorption spectra, and natural transition orbitals. See DOI:10.1039/x0xx00000x

molecular processes; and (3) low emission quantum yields and short-lived triplet excited states induced by the bridging ligand-facilitated nonradiative processes.³⁰⁻³⁵ However, the feasible intramolecular π - π and/or metal-metal interactions in dinuclear complexes are expected to alter the nature and energy of the singlet and triplet excited states, promoting special photophysical features. In particular, studies on a variety of dinuclear Ir(III) complexes linked by N[^]N, C[^]N, or N[^]O-ligands revealed that π -conjugation in the bridging ligand resulted in a bathochromic shift in their absorption and emission spectra with respect to their mononuclear counterparts.³⁶ This feature was attributed to the participation of the bridging ligand-based π , π^* or intraligand charge transfer (ILCT) configurations in the excited states³⁷⁻⁴⁰ or lowering of the metal-to-ligand charge transfer (MLCT) / ligand-to-ligand charge transfer (LLCT) excited states due to the enhanced electron-withdrawing capability of the bridging ligand.⁴¹ The presence of bridging ligand-based transitions also enhanced the two-photon absorption³⁷ and electrochemiluminescence⁴² of the dinuclear complexes. Moreover, our group and the other groups have revealed the enhanced photocytotoxicities of the dinuclear Ir(III) complexes for *in vitro* photodynamic therapy of cancer cells compared to their mononuclear counterparts.⁴³ Therefore, the unique photophysical properties and potential applications of the dinuclear Ir(III) complexes are worthy of further study.

Among the variety of applications of Ir(III) complexes, optical limiting (OPL) based on reverse saturable absorption (RSA, *i.e.* a nonlinear optical phenomenon that exhibits an increased absorptivity upon increasing the incident fluence) is underexplored. The readily populated triplet excited state due to heavy Ir metal induced rapid intersystem crossing and the broad and relatively strong triplet excited-state absorption of Ir(III) complexes make them attractive candidates as reverse saturable absorbers for OPL applications. Our group and other groups have extensively investigated the RSA of various mononuclear Ir(III) complexes.²³⁻²⁹ However, the study on RSA of dinuclear Ir(III) complexes is sparse.

For a broadband RSA material, it is desirable to have a broad but weak ground-state absorption in the visible to the near-IR region where the excited-state absorption is strong. Meanwhile the material is expected to possess long-lived triplet excited state for broad temporal response. However, it has remained to be a challenge to red-shift the ground-state absorption while keeping a long-lived triplet excited state.⁴⁴ This dilemma arises from the fact that red-shifting the ground-state absorption to longer wavelengths requires a low-lying singlet excited state, which leads to an even lower triplet excited state typically exhibiting a rapid nonradiative decay. Therefore, the reported lifetimes of the lowest triplet excited state are significantly shortened in Ir(III) complexes with red-shifted charge-transfer absorption to the red/NIR spectral regions,^{10,11,24,25,29,45} which weakens their triplet excited-state absorption and limits their application as broadband reverse saturable absorbers. An example of this dilemma is the Ir(III) complexes with the 2-(2-quinolinyl)quinoxaline (quqo, structure shown in Chart 1) ligand, in which the charge-transfer absorption band was red-shifted to 730 nm while the T_1 lifetime was too short (ps range) to allow for their ns transient absorption to be detected.¹¹ To remedy this deficiency, we extended the π -conjugation of the quqo ligand *via* incorporating fluorenyl

substituents (Chart 1) on the quqo ligand, which prolonged the T_1 lifetimes of the mononuclear Ir(quqo)(piq)₂⁺ (piq refers to 1-phenylisoquinoline, Chart 1) complexes and significantly improved the triplet excited-state absorption.⁴⁶

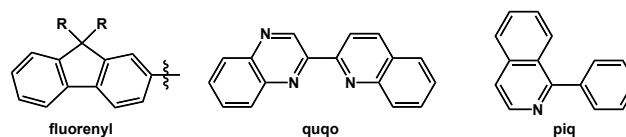


Chart 1 Structures of fluorenyl substituent, quqo and piquo.

Inspired by the promising RSA results from the mononuclear Ir(quqo)(piq)₂⁺ complexes with π -expansive diimine ligand and the aforementioned interesting properties of the dinuclear Ir(III) complexes, we tethered two Ir(quqo)(piq)₂⁺ complexes by a fluorenyl linker, aiming to realize weak ground-state absorption but strong and broad excited-state absorption in the visible to the near-IR regions meanwhile retaining a reasonably long-lived triplet excited state for broadband RSA based optical limiting applications. Therefore, two dinuclear Ir(III) complexes with fluorenyl-tethered quqo ligands were synthesized (**Ir-1** and **Ir-2** in Scheme 1). The photophysical properties of these two complexes were systematically investigated with UV-vis absorption, emission and transient absorption spectroscopy and simulated by TDDFT calculations. The RSA of these two complexes was demonstrated at 532 nm for ns laser pulses.

Experimental section

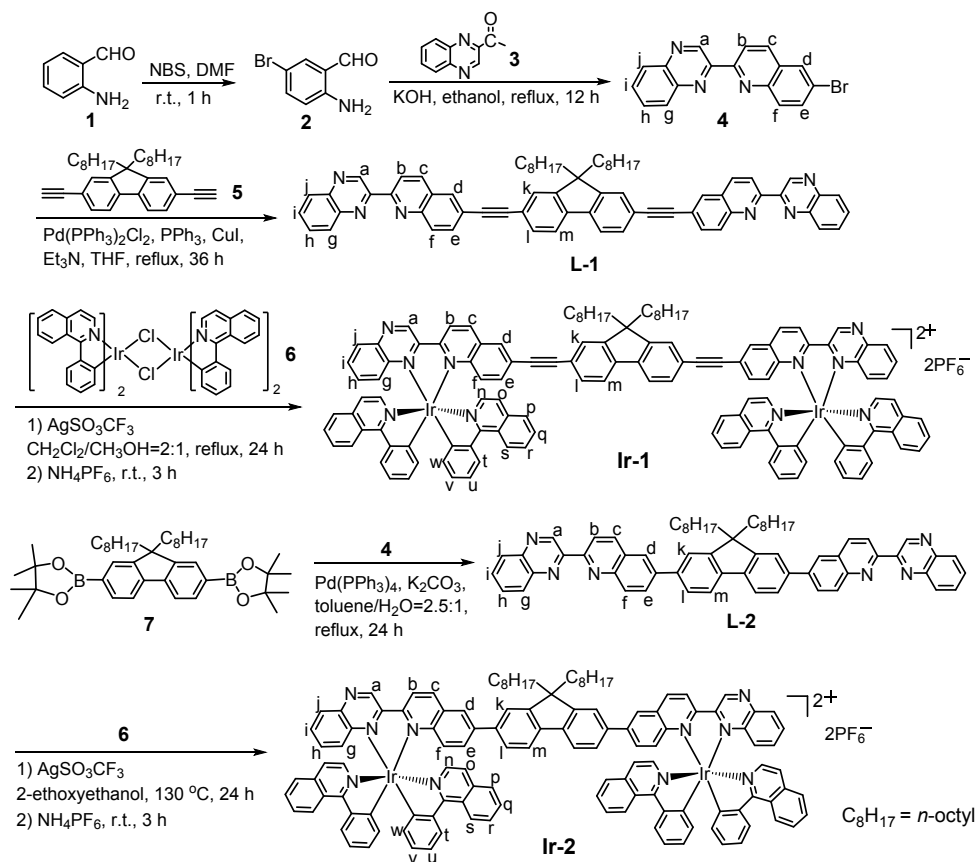
Synthesis and characterization

All reagents and solvents for synthesis were purchased from Aldrich or Alfa Aesar and used as received unless otherwise stated. Precursors **5**,⁴⁷ **6**,²⁷ and **7**²⁸ were prepared according to the procedures previously reported by our group. Tetrahydrofuran (THF) and triethylamine (Et₃N) were distilled under N₂ over sodium benzophenone ketyl. Silica gels (230–400 mesh) used for chromatography were purchased from Alfa Aesar. The intermediate compounds were characterized by ¹H NMR spectroscopy, while the ligands **L-1** and **L-2**, and complexes **Ir-1** and **Ir-2** were characterized by ¹H NMR, HRMS, and elemental analyses. ¹H NMR spectra were recorded on a Varian Oxford-400 or Oxford-500 VNMR spectrometer. ESI-HRMS analyses were performed on a Bruker BioTOF III mass spectrometer. Elemental analyses were carried out by NuMega Resonance Laboratories, Inc. in San Diego, California. The synthetic details and characterization data for compound **4**, ligands **L-1** and **L-2**, and complexes **Ir-1** and **Ir-2** are given below, and their ¹H NMR spectra are provided in ESI Fig. S1.

Compound 4. To a solution of 2-aminobenzaldehyde **1** (300 mg, 2.48 mmol) in DMF (20 mL) was added NBS (440 mg, 2.48 mmol), and the solution was stirred at r.t. for 1 h. After that, the yellow solution was poured into water and extracted with CH₂Cl₂. Then the organic layer was washed with water, dried over anhydrous Na₂SO₄, and evaporated under reduced pressure to obtain the crude product **2** as yellow needles. The obtained crude product **2** was used immediately for the following step reaction without further purification. Saturated ethanol solution of KOH (20 mL) was added

to the mixture of compounds **2** and **3** (385 mg, 2.23 mmol) and refluxed for 12 h. After cooling to r.t, water was added to the reaction mixture and the precipitate was collected by filtration to get the crude product **4**, which was purified by column chromatography on silica gel (hexane/ethyl acetate = 8/1, v/v) to

obtain yellow powder (500 mg, yield: 67%). ^1H NMR (400 MHz, CDCl_3): δ 10.16 (s, 1H, H_a), 8.76 (d, $J = 8.8$ Hz, 1H, H_c), 8.24 (d, $J = 8.5$ Hz, 1H, H_f), 8.20-8.14 (m, 2H, H_g/H_j), 8.11 (d, $J = 8.8$ Hz, 1H, H_b), 8.04 (d, $J = 2.0$ Hz, 1H, H_d), 7.85-7.82 (dd, $J = 8.5, 2.0$ Hz, 1H, H_e), 7.82-7.78 (m, 2H, H_h/H_i).



Scheme 1 Synthetic routes and structures for complexes **Ir-1** and **Ir-2**.

Ligand L-1. A stirred mixture of compounds **4** (253 mg, 0.752 mmol), **5** (150 mg, 0.342 mmol), PPh_3 (36 mg, 0.068 mmol), $\text{Pd(PPh}_3)_2\text{Cl}_2$ (48 mg, 0.068 mmol), CuI (13 mg, 0.068 mmol), Et_3N (6 mL) and THF (25 mL) was purged with nitrogen and heated to reflux for 36 h. The mixture was cooled to r.t. and the solvent was removed. The residue was washed with brine and the solid was dissolved in CH_2Cl_2 . The CH_2Cl_2 layer was then dried over anhydrous Na_2SO_4 and the solvent was removed. The residue was purified by column chromatography on silica gel (hexane/toluene/ethyl acetate = 31/31/1, v/v) to give **L-1** as a yellow solid (80 mg, yield: 24%). ^1H NMR (500 MHz, CDCl_3): δ 10.23 (s, 2H, H_a), 8.79 (d, $J = 8.5$ Hz, 2H, H_c), 8.33 (d, $J = 8.5$ Hz, 2H, H_f), 8.26 (d, $J = 8.5$ Hz, 2H, H_b), 8.24-8.18 (m, 4H, H_g/H_j), 8.15-8.10 (m, 2H, H_d), 7.96-7.91 (m, 2H, H_m), 7.86-7.79 (m, 4H, H_k/H_l), 7.75 (d, $J = 8.5$ Hz, 2H, H_e), 7.68-7.60 (m, 4H, H_h/H_i), 2.13-2.03 (m, 4H, $\text{CH}_2(\text{CH}_2)_6\text{CH}_3$), 1.05-0.56 (m, 30H, $\text{CH}_2(\text{CH}_2)_6\text{CH}_3$). ESI-HRMS: m/z Calcd for $[\text{C}_{67}\text{H}_{60}\text{N}_6+\text{H}]^+$, 949.4958; found: 949.4936. Anal. Calcd (%) for $\text{C}_{67}\text{H}_{60}\text{N}_6 \cdot 0.5\text{H}_2\text{O}$: C, 83.98; H, 6.42; N, 8.77. Found: C, 84.31; H, 6.83; N, 8.79.

Complex Ir-1. To a stirred solution of compounds **6** (100 mg, 0.115 mmol) and **L-1** (50 mg, 0.078 mmol) in degassed $\text{CH}_2\text{Cl}_2/\text{MeOH}$ (30 mL, 2/1, v/v) was added AgSO_3CF_3 (30 mg, 0.115

mmol). The mixture was refluxed for 24 h under nitrogen. After cooling to r.t., 10-fold NH_4PF_6 was added. The suspension was stirred at r.t. for 3 h and then filtered to remove any insoluble salts. After removal of the solvent, the crude product was purified by column chromatography on silica gel ($\text{CH}_2\text{Cl}_2/\text{ethyl acetate} = 30/1$, v/v) to afford **Ir-1** as a brownish-green solid (50 mg, yield: 34%). ^1H NMR (500 MHz, CDCl_3): δ 10.04 (s, 2H, H_a), 8.92-8.89 (d, $J = 8.5$ Hz, 2H, H_c), 8.88-8.79 (m, 4H, H_n), 8.66 (d, $J = 8.5$ Hz, 2H, H_f), 8.26 (d, $J = 7.5$ Hz, 4H, H_t), 8.13-8.08 (d, $J = 8.5$ Hz, 2H, H_b), 8.08-8.02 (s, br. 2H, H_d), 7.90-7.47 (m, 28H, $\text{H}_{e,g,h,i,j,k,l,m,o,p,s}$), 7.33 (t, $J = 6.5$ Hz, 4H, H_q), 7.25-7.10 (m, 8H, H_u/H_w), 6.92 (t, $J = 7.0$ Hz, 4H, H_r), 6.42-6.38 (dd, $J = 7.0, 14.0$ Hz, 4H, H_v), 2.08-1.94 (m, 4H, $\text{CH}_2(\text{CH}_2)_6\text{CH}_3$), 0.98-0.47 (m, 30H, $\text{CH}_2(\text{CH}_2)_6\text{CH}_3$). ESI-HRMS: m/z Calcd for $[\text{C}_{127}\text{H}_{100}\text{Ir}_2\text{N}_{10}]^{2+}$, 1075.3707; found, 1075.3723. Anal. Calcd (%) for $\text{C}_{127}\text{H}_{100}\text{Ir}_2\text{N}_{10}\text{P}_2 \cdot 2\text{CHCl}_3 \cdot 2\text{CH}_2\text{Cl}_2 \cdot 0.5\text{C}_6\text{H}_{14}$: C, 55.65; H, 3.94; N, 4.84. Found: C, 55.58; H, 4.25; N, 5.09.

Ligand L-2. A stirred mixture of compounds **4** (196 mg, 0.582 mmol), **7** (170 mg, 0.265 mmol), K_2CO_3 (3.4 g, 24.6 mmol), $\text{Pd(PPh}_3)_4$ (61.2 mg, 0.053 mmol), toluene (25 mL) and H_2O (10 mL) was purged with nitrogen and heated to reflux for 24 h. The mixture was cooled to r.t., poured into water, and extracted with ethyl acetate.

The organic layer was dried over anhydrous Na_2SO_4 and the solvent was removed. The residue was purified by column chromatography on silica gel (hexane/ethyl acetate = 20/1 - 10/1, v/v) to give **L-2** as a yellow solid (105 mg, yield: 44%). ^1H NMR (500 MHz, CDCl_3): δ 10.28 (s, 2H, H_a), 8.82 (d, $J = 8.5$ Hz, 2H, H_c), 8.45 (d, $J = 8.5$ Hz, 2H, H_f), 8.38 (d, $J = 8.5$ Hz, 2H, H_b), 8.27-8.20 (m, 4H, H_g/H_i), 8.16-8.12 (m, 4H, H_d/H_m), 7.91 (d, $J = 8.5$ Hz, 2H, H_e), 7.87-7.78 (m, 8H, $\text{H}_k/\text{H}_l/\text{H}_n/\text{H}_j$), 2.25-2.15 (m, 4H, $\text{CH}_2(\text{CH}_2)_6\text{CH}_3$), 1.05-0.58 (m, 30H, $\text{CH}_2(\text{CH}_2)_6\text{CH}_3$). ESI-HRMS: m/z Calcd for $[\text{C}_{63}\text{H}_{60}\text{N}_6+\text{H}]^+$, 901.4958; found, 901.5004. Anal. Calcd (%) for $\text{C}_{63}\text{H}_{60}\text{N}_6 \cdot 0.05\text{CH}_2\text{Cl}_2$: C, 83.64; H, 6.69; N, 9.28. Found: C, 83.47; H, 7.08; N, 9.39.

Complex Ir-2. Compounds **6** (159 mg, 0.125 mmol), **L-2** (75 mg, 0.083 mmol), and AgSO_3CF_3 (32 mg, 0.125 mmol) were added to degassed 2-ethoxyethanol (20 mL) and heated to 130 °C under nitrogen for 24 h. The reaction mixture was cooled to r.t. and 10-fold NH_4PF_6 was added. The suspension was stirred at r.t. for 3 h and then filtered to remove any insoluble salts. After removal of the solvent, the crude product was purified by column chromatography on silica gel (CH_2Cl_2 /ethyl acetate = 40/1 - 10/1, v/v) to give **Ir-2** as a greenish-brown solid (70 mg, yield: 35%). ^1H NMR (500 MHz, CDCl_3): δ 10.06 (s, 2H, H_a), 8.98-8.74 (m, 8H, $\text{H}_c/\text{H}_f/\text{H}_n$), 8.31-8.21 (m, 4H, H_t), 8.14-8.04 (m, 4H, H_b/H_d), 7.90-7.53 (m, 28H, $\text{H}_{e,g,h,i,j,k,l,m,o,p,s}$), 7.41-7.22 (m, $J = 7.5$ Hz, 8H, H_q/H_w), 7.14 (t, $J = 7.5$ Hz, 4H, H_u), 6.92 (t, $J = 7.5$ Hz, 4H, H_r), 6.45-6.35 (dd, $J = 7.5, 9.8$ Hz, 4H, H_v), 2.15-2.00 (m, 4H, $\text{CH}_2(\text{CH}_2)_6\text{CH}_3$), 0.95-0.48 (m, 30H, $\text{CH}_2(\text{CH}_2)_6\text{CH}_3$). ESI-HRMS: m/z Calcd for $[\text{C}_{123}\text{H}_{100}\text{Ir}_2\text{N}_{10}]^{2+}$, 1051.3707; found, 1051.3740. Anal. Calcd (%) for $\text{C}_{123}\text{H}_{100}\text{F}_{12}\text{Ir}_2\text{N}_{10}\text{P}_2$: C, 61.75; H, 4.21; N, 5.85. Found: C, 61.72; H, 4.60; N, 6.06.

Photophysical measurements.

Spectroscopic grade solvents from VWR International were used for the photophysical studies without further purification. The UV-vis absorption spectra were recorded on a Shimadzu UV-2501 spectrophotometer and the steady-state emission spectra were obtained on a Jobin-Yvon FluoroMax-4 fluorometer/phosphorometer. The emission quantum yields were determined by the relative actinometry method⁴⁸ in different solvents (the solutions of **Ir-1** and **Ir-2** were degassed with argon for 40 min), in which a degassed acetonitrile solution of $[\text{Ru}(\text{bpy})_3]\text{Cl}_2$ ($\Phi_{\text{em}} = 0.097$, $\lambda_{\text{ex}} = 436$ nm)⁴⁹ was used as the reference for complexes **Ir-1** and **Ir-2**, and a 1 N sulfuric acid solution of quinine bisulfate ($\Phi_{\text{em}} = 0.546$, $\lambda_{\text{ex}} = 347.5$ nm)⁵⁰ was used as the reference for ligands **L-1** and **L-2**. The nanosecond transient absorption (TA) spectra and triplet lifetimes were measured in argon-sparged (40 min) CH_2Cl_2 solutions for **L-1** and **L-2**, and in CH_3CN solutions for **Ir-1** and **Ir-2** on an Edinburgh LP920 laser flash photolysis spectrometer. The third harmonic output (355 nm) of a Nd:YAG laser (Quantel Brilliant, pulse duration = 4.1 ns; repetition rate = 1 Hz) was employed as the pump beam. The triplet excited-state absorption coefficients (ϵ_T) at the TA band maxima were determined by the singlet depletion method,⁵¹ and the triplet excited state quantum yields were calculated by the relative actinometry⁵² with SiNc in benzene solution ($\epsilon_{590} = 70,000$ L mol⁻¹ cm⁻¹, $\Phi_T = 0.20$)⁵³ as the reference.

Nonlinear transmission measurements

The RSA of complexes **Ir-1** and **Ir-2** was demonstrated by nonlinear transmission experiment at 532 nm using a Quantel Brilliant laser (pulse width = 4.1 ns, repetition rate = 10 Hz) as the light source. **Ir-1** and **Ir-2** were dissolved in CH_2Cl_2 and the concentrations of the sample solutions were adjusted to obtain a linear transmission of 80% at 532 nm in a 2-mm cuvette. The experimental setup and details were similar to those reported previously.²⁴ The focal length of the plano-convex lens was 40 cm, and the radius of the beam waist at the focal point was approximately 96 μm .

Computational methods

Geometries of the Ir(III) complexes and ligands were optimized at the level of density functional theory (DFT) implemented in Gaussian09 software package.⁵⁴ The electronic structure calculations were carried out with Douglas-Kroll-Hess approximation.^{55,56} The absorption energies were calculated using time-dependent DFT (TDDFT) by iteratively solving the eigenvalue equation based on Davidson algorithm.⁵⁷⁻⁵⁹ Absorption spectra were plotted based on inhomogeneous Gaussian line-broadening of 50 optical transitions calculated by TDDFT. The ΔSCF approach was employed to obtain the phosphorescence energies based on the triplet ground-state geometries optimized using unrestricted DFT method and the lowest triplet transition energies were obtained by TDDFT calculations.

The hybrid PBE1 functional⁶⁰ and the mixed basis set with LANL2DZ for Ir and 6-31G* for the remaining atoms were used for the ground- and excited-state calculations. All calculations were performed using conductor-like polarizable continuum model (CPCM),⁶¹ as implemented in Gaussian09. For **Ir-1** and **Ir-2**, CH_3CN was used as the solvent media, while CH_2Cl_2 was used as the solvent media for **L-1** and **L-2** to be consistent with the experimental condition. The phosphorescence energies were estimated in solvent according to the state-specific approach,⁶² which accounts for the non-equilibrium effect of slow component of reaction field of solvent. Natural transition orbital (NTO)⁶³ analysis was performed to characterize each excitation as a hole-electron pair by applying unitary transformation of transition density matrix of a specific excited state. Chemcraft-1.7 software⁶⁴ was used for plotting the ground- and excited-state charge densities by setting the isovalue as 0.02.

Results and discussion

Electronic absorption

The UV-Vis absorption of **L-1**, **L-2**, **Ir-1** and **Ir-2** was investigated in different solvents and the concentration-dependency studies were conducted for **L-1** and **L-2** in CH_2Cl_2 and **Ir-1** and **Ir-2** in CH_3CN in a concentration range of 1×10^{-6} - 1×10^{-4} mol L⁻¹. The experimental absorption spectra of **L-1** and **L-2** in CH_2Cl_2 and **Ir-1** and **Ir-2** in CH_3CN are presented in Fig. 1a. The absorption band maxima and molar extinction coefficients are listed in Table 1. The absorption of these compounds followed the Beer's law, indicating the absence of ground-state aggregation in the tested concentration range. The absorption spectra of **L-1**, **L-2**, **Ir-1** and **Ir-2** were simulated by TDDFT and the results are displayed in Fig. 1b. The energies, shapes, and relative intensities of the calculated spectra agreed well with the experimental ones (ESI Fig. S2). The natures of the low-energy

and most intensive optical transitions are represented by their NTOs shown in Tables 2 and S1.

The absorption spectra of ligands **L-1** and **L-2** are composed of a major absorption band at 350-450 nm that is broad, less structured, and strong. Considering the large molar extinction coefficients of this band and the π -conjugation nature of these two ligands, this band is attributed predominantly to ${}^1\pi,\pi^*$ transitions, likely mixed with some intramolecular charge transfer (1 ICT) character in view of the electron-withdrawing capability of quqo. This attribution is supported by the NTOs for the S_1 states of these two ligands (see Table 2), for which the holes are mainly distributed on the bridging fluorenyl motif and extended to the quinolinyl groups, while the electrons are delocalized over the entire molecule. Because of the extended π -conjugation induced by the two $C\equiv C$ bonds in **L-1**, the absorption bands of **L-1** are slightly red-shifted in comparison to those of **L-2**.

The complexes **Ir-1** and **Ir-2** displayed strong absorption bands at ca. 320-400 nm, and broad and featureless absorption bands at 400-540 nm. With reference to the NTOs shown in Table 2, the low-energy band at 400-540 nm is ascribed predominantly to the 1 ILCT transition from the π -donating bridging fluorenyl motif to electron-accepting quqo ligands, admixing with minor ${}^1\pi,\pi^*$ character. In comparison to the ${}^1\pi,\pi^*$ / 1 ILCT bands in their corresponding ligands, the 1 ILCT/ ${}^1\pi,\pi^*$ bands in the complexes are broader, weaker and bathochromically shifted. This change should be attributed to the increased 1 ILCT contribution in the complexes due to the enhanced electron-withdrawing ability of quqo after complexation with Ir(III) ions. Meanwhile, the 3 MLCT/ 3 LLCT transitions associated with one of the metal centers contributed to the lower-energy end of this absorption bands at ~ 500 nm. Based on the NTOs in Table S1, the

other strong absorption band at ca. 330 nm also has the predominant 1 ILCT/ ${}^1\pi,\pi^*$ / 1 MLCT character, but the electrons are much less delocalized compared to the low-energy transitions.

In addition to the aforementioned absorption bands, **Ir-1** and **Ir-2** possess a broad but very weak band at ca. 540-700 nm (see the inset in Fig. 1a). With reference to the other reported Ir(III) complexes especially those bearing quqo ligand, this band can be assigned to spin-forbidden 3 MLCT/ 3 LLCT/ ${}^3\pi,\pi^*$ transitions.^{10,11,25,46,65}

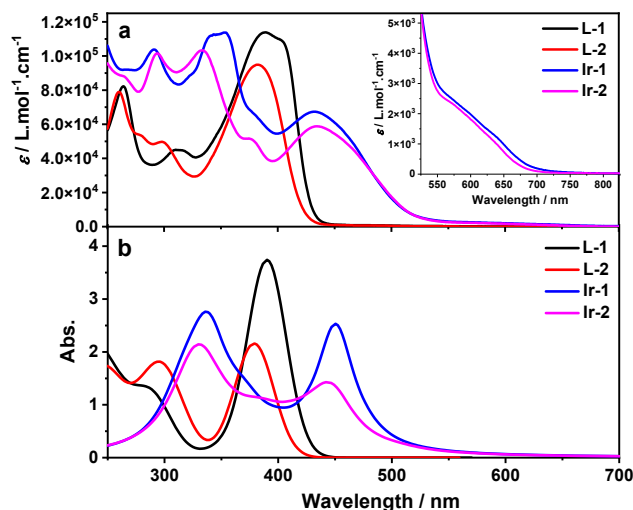


Fig. 1 (a) Experimental and (b) calculated absorption spectra of **L-1** and **L-2** in CH_2Cl_2 and **Ir-1** and **Ir-2** in CH_3CN . The inset in panel (a) shows the expansion of the experimental spectra at 525-825 nm.

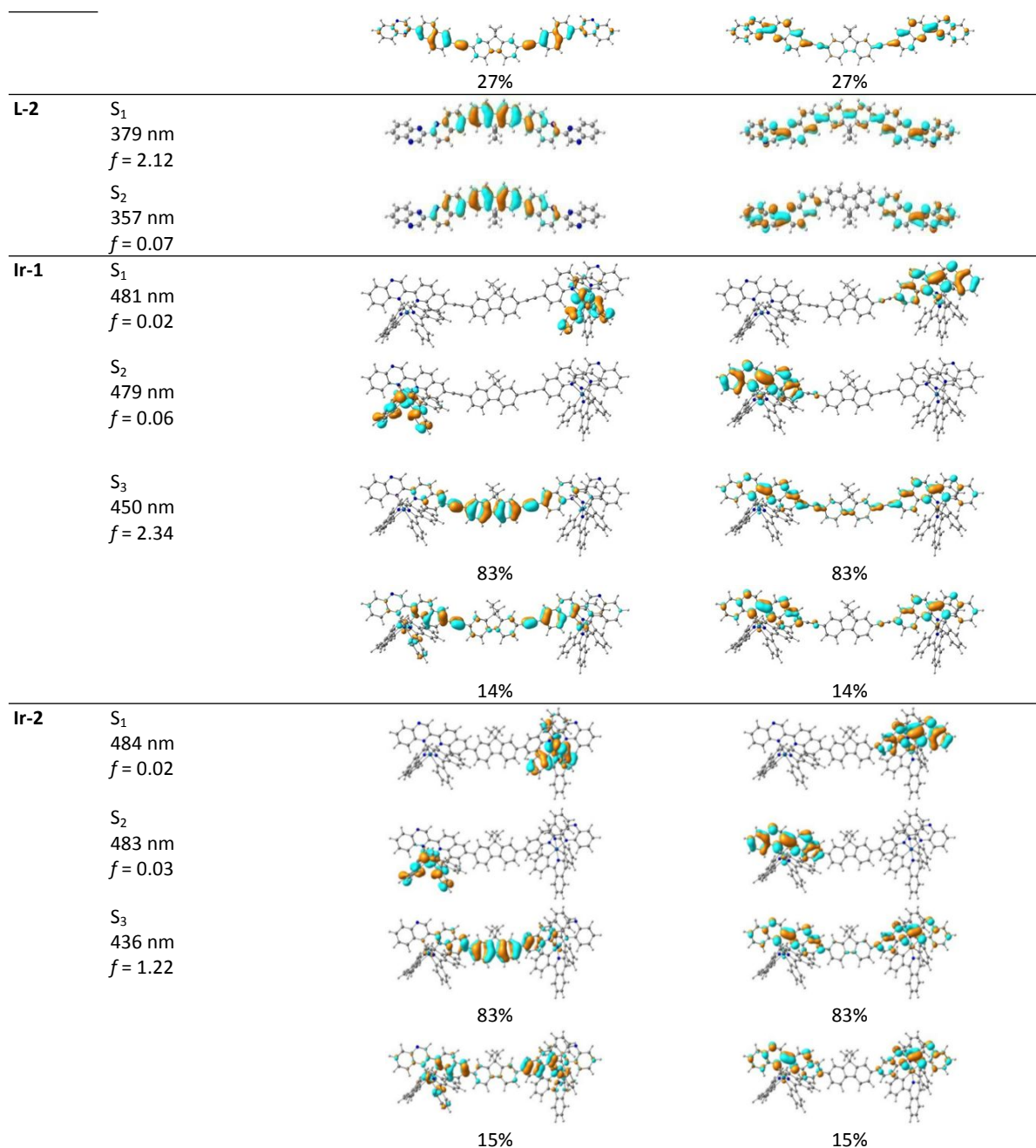
Table 1 Electronic absorption, emission, and triplet excited-state absorption parameters of **L-1** and **L-2** in CH_2Cl_2 and **Ir-1** and **Ir-2** in CH_3CN .

	λ_{abs}/nm ($\epsilon/10^4$ L mol $^{-1}$ cm $^{-1}$) ^a	λ_{em}/nm (τ_{em}/ns); Φ_{em} ^b	λ_{T1-Tn}/nm (τ_T/ns , $\epsilon_{T1-Tn}/10^4$ L mol $^{-1}$ cm $^{-1}$); Φ_T ^c
L-1	311 (4.42), 390 (11.37)	472 (-); 0.67	500 (28820, 4.98); 0.093
L-2	298 (4.78), 382 (9.39)	477 (-); 0.64	506 (24870, 3.40); 0.15
Ir-1	292 (10.40), 353 (11.42), 432 (6.76), 555 (0.29)	590 (1420), 618 (1220), 700 (40 (20%), 1320 (80%)); 0.003	520 (40, 6.91); 0.072
Ir-2	294 (10.15), 334 (10.33), 434 (5.88), 555 (0.25)	588 (2490), 716 (60); 0.003	512 (50, 5.92); 0.23

^aAbsorption band maxima (λ_{abs}) and molar extinction coefficients (ϵ) at room temperature. ^bEmission band maxima (λ_{em}) and quantum yields (Φ_{em}) at room temperature with Ru(bpy) $_3$ Cl $_2$ in degassed CH_3CN ($\Phi_{em} = 0.097$, $\lambda_{ex} = 436$ nm) as the reference for complexes **Ir-1** and **Ir-2** and a 1 N sulfuric acid solution of quinine bisulfate ($\Phi_{em} = 0.546$, $\lambda_{ex} = 347.5$ nm) as the reference for ligands **L-1** and **L-2**. The lifetimes of **Ir-1** and **Ir-2** were measured at $c = 1 \times 10^{-5}$ mol.L $^{-1}$. The lifetimes of **L-1** and **L-2** were too short to be measured on our instrument. ^cNanosecond TA band maxima (λ_{T1-Tn}), triplet excited-state lifetimes (τ_T), triplet extinction coefficients (ϵ_{T1-Tn}), and triplet quantum yields (Φ_T) measured at room temperature with SiNc in benzene ($\epsilon_{590\text{ nm}} = 70,000$ L mol $^{-1}$ cm $^{-1}$, $\Phi_{em} = 0.20$) as the reference.

Table 2 Natural transition orbitals (NTOs) representing the low-energy transitions for **L-1** and **L-2** in CH_2Cl_2 and **Ir-1** and **Ir-2** in CH_3CN .

States and Properties		Hole	Electron
L-1	S_1 390 nm $f = 3.73$		
	S_2 351 nm $f = 0.17$	 68%	 68%



Photoluminescence

The emission characteristics of **L-1**, **L-2**, **Ir-1** and **Ir-2** were investigated in different solvents at room temperature. The normalized room-temperature emission spectra of **L-1** and **L-2** in CH_2Cl_2 , and **Ir-1** and **Ir-2** in CH_3CN at a concentration of 1×10^{-5} mol L^{-1} are displayed in Fig. 2, and the spectra in different solvents are provided in Fig. S4. The emission parameters are summarized in Tables 1 and S2. As shown in Fig. 2, **L-1** and **L-2** exhibit a structureless blue emission in CH_2Cl_2 , which shows a positive solvatochromic effect in more polar solvents like acetone and acetonitrile (Fig. S4). The featureless spectra, their insensitivity to air and short lifetimes (< 10 ns), along with the positive solvatochromic effect suggest that the emission of **L-1** and **L-2** in these polar solvents is fluorescence arising from an ^1ICT state,¹⁹ which is supported by the NTOs of the calculated singlet emitting

states (Table S3). In nonpolar or less polar solvents like hexane and toluene, the fluorescence spectra become much narrower, vibronically resolved, and blue-shifted, implying a $^1\pi, \pi^*$ emission. Switching the emitting state from a charge transfer state to a $^1\pi, \pi^*$ state when solvent polarity decreases is a common feature for molecules composing an acceptor-donor structure.¹⁹

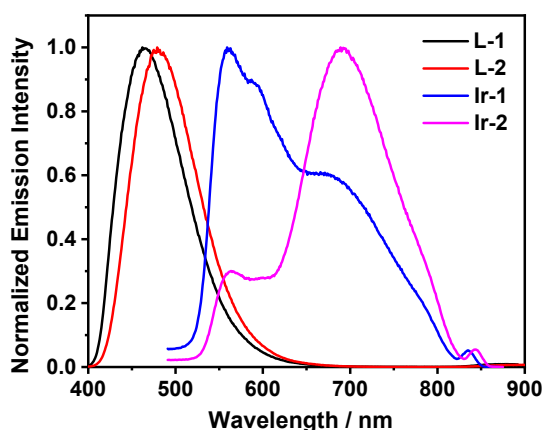


Fig. 2 Normalized emission spectra of **L-1** and **L-2** in CH_2Cl_2 , and **Ir-1** and **Ir-2** in CH_3CN . The excitation wavelength was 390 nm for **L-1**, 382 nm for **L-2**, 432 nm for **Ir-1**, and 434 nm for **Ir-2**. The concentration used was $1 \times 10^{-5} \text{ mol L}^{-1}$.

The emission of complexes **Ir-1** and **Ir-2** shows a significant red-shift in comparison to their excitation wavelengths, and the

emission is prone to oxygen quenching. These characteristics are consistent with phosphorescence from a triplet excited state. Both complexes exhibit dual emission. With reference to the complexes that possess quqo ligand, the low-energy emission band at $\geq 700 \text{ nm}$ can be ascribed to a ${}^3\text{MLCT} (d(\text{Ir}) \rightarrow \pi^*(\text{quqo})) / {}^3\text{LLCT} (\pi(\text{piq}) \rightarrow \pi^*(\text{quqo}))$ state,^{11,22,35,46} while the high-energy emission band at 587 nm is attributed to the fluorenyl-linked quqo ligand-localized ${}^3\pi, \pi^* / {}^3\text{CT}$ emission with reference to our previous reported Ir(III) complexes with donor-acceptor character.³⁵ For complex **Ir-1**, the extended π -conjugation in N^N ligand causes a stronger high-energy emission in comparison to that of **Ir-2**, indicating a stronger contribution of the ${}^3\pi, \pi^*$ configuration to the high-energy emitting state.

The dual emission and charge transfer nature of the emitting states for **Ir-1** and **Ir-2** are supported by the TDDFT calculations. As the NTOs in Table 3 manifest, the low-energy emitting states for both complexes are ${}^3\text{MLCT}/{}^3\text{LLCT}$ transitions in nature; while the high-energy emission has a predominant ${}^3\pi, \pi^* / {}^3\text{ILCT}$ character, admixing with some ${}^3\text{MLCT}/{}^3\text{LLCT}$ characters.

Table 3 NTOs corresponding to the triplet emitting states for **Ir-1** and **Ir-2** in CH_3CN .

	Emission energy	Electron	Hole
Ir-1	735 nm		
	594 nm		
		65%	65%
	17%	17%	
Ir-2	722 nm		
	634 nm		
		51%	51%
	11%	11%	

The emission of **Ir-1** and **Ir-2** in other solvents (hexane, toluene, CH_2Cl_2 , and acetone) was also studied. As shown in Fig. S4, the relative intensity of the high-energy emission band decreases or disappears in these solvents in comparison to that in CH_3CN , likely due to the decreased charge transfer character of this emitting excited state when the polarity of the solvent decreases, which is in line with the significant ${}^3\text{ILCT}$ character of this emitting state.

Meanwhile, the phosphorescence quantum yields of these two complexes in both polar and nonpolar solvents are very low, which is a common feature for dinuclear Ir(III) complexes.³⁵ Another general trend revealed is that the high-energy emission band in **Ir-2** is much weaker or absent in each corresponding solvent comparing to those of **Ir-1**, supporting the less ${}^3\pi, \pi^*$ contribution to

this band in **Ir-2** due to the shorter π -conjugation of the bridging ligand in this complex with respect to that in **Ir-1**.

Transient absorption

The nanosecond transient absorption (TA) spectra of **L-1** and **L-2** in CH_2Cl_2 and **Ir-1** and **Ir-2** in CH_3CN were studied to further understand the triplet excited-state characteristics. The TA spectra at zero delay after 355-nm excitation are shown in Fig. 3, and the TA parameters, i.e. the TA band maxima, the triplet excited-state lifetimes by monitoring the decay of TA signals, the triplet excited-state molar extinction coefficients, and the triplet excited-state quantum yields are listed in Table 1. The time-resolved TA spectra of **L-1**, **L-2**, **Ir-1**, and **Ir-2** are provided in ESI Fig. S5.

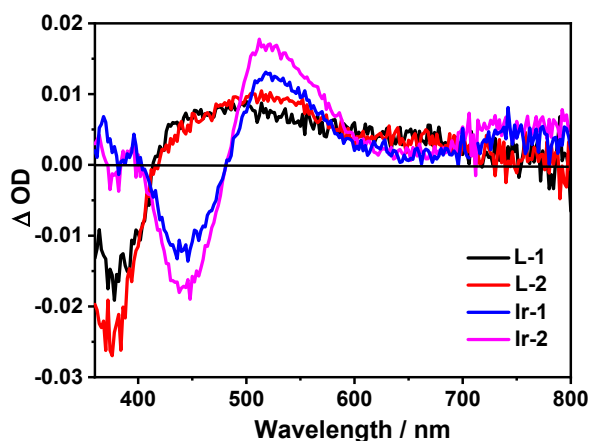


Fig. 3 Nanosecond TA spectra of **L-1** and **L-2** in CH_2Cl_2 , and **Ir-1** and **Ir-2** in CH_3CN at zero delay after 355-nm excitation. $A_{355} = 0.4$ in a 1 cm cuvette.

Ligands **L-1** and **L-2** display quite similar TA spectra, with a broad positive TA band at 420–700 nm and bleaching occurring below 420 nm that are in line with their $^1\pi,\pi^*$ absorption bands. In view of the long triplet lifetimes, the observed TA of **L-1** and **L-2** is attributed to their $^3\pi,\pi^*$ state. For complexes **Ir-1** and **Ir-2**, their bleaching bands appear at ca. 450 nm, which are consistent with the $^1\text{MLCT}/^1\pi,\pi^*$ absorption bands in their respective UV-vis spectra. In comparison to the TA spectra of their corresponding ligands, the TA spectra of the complexes exhibit much stronger signals in the regions of 490–600 nm and 700–800 nm. However, the deduced triplet lifetimes of **Ir-1** and **Ir-2** are much shorter than those of their corresponding ligands but are in accordance with the emission lifetimes deduced from the low-energy $^3\text{MLCT}/^3\text{LLCT}$ emission band. These characteristics imply that the transient absorbing excited states of **Ir-1** and **Ir-2** are likely the emitting $^3\text{MLCT}/^3\text{LLCT}$ excited states. The spectral features and lifetimes of these two complexes resemble those of the dinuclear Ir(III) quqo complex tethered by a carbazolyl motif.³⁵

Comparison of the TA characteristics of **Ir-1** and **Ir-2** reveals that extending the π -conjugation of the bridging ligand in **Ir-1** causes a slight redshift of the TA band maximum with respect to that of **Ir-2**. However, the ΔOD values at the positive absorption band 490–600 nm for **Ir-1** are slightly smaller than those of **Ir-2**, presumably being ascribed to its slightly stronger ground-state absorption in this spectral region. The triplet excited-state lifetimes for both

complexes are quite similar, but the triplet excited-state formation quantum yield of **Ir-1** is lower than that of **Ir-2**. These characteristics are different from what was discovered in the mononuclear Ir(III) complexes, in which extending the π -conjugation of the $\text{N}^{\wedge}\text{N}$ ligands prolonged the triplet excited-state lifetime and improved the triplet excited-state absorption via admixing the $\text{N}^{\wedge}\text{N}$ ligand-localized $^3\pi,\pi^*$ character into the transient absorbing T_1 state.^{24–28,46} This difference confirms that the transient absorbing excited states in **Ir-1** and **Ir-2** are not delocalized to the bridging ligand, instead they are localized excited states originated from the same structural feature and share the same nature, i.e. the $^3\text{MLCT}/^3\text{LLCT}$ state.

Reverse saturable absorption (RSA)

RSA, a nonlinear absorption process in which the absorptivity increases with the increased incident fluence, is expected to occur when the excited-state absorption is stronger than the ground-state absorption at an interested wavelength. RSA can be employed for optical limiting,^{10,11,19,23–28,46} optical switching,⁶⁶ optical rectification,⁶⁷ laser beam compression, stabilization, and modulation.⁶⁸ The positive absorption bands at 490–800 nm in the TA spectra of **Ir-1** and **Ir-2** clearly indicate a stronger excited-state absorption compared to the ground-state absorption in this spectral region. Thus, RSA is anticipated to occur from these complexes in this spectral region. To verify this phenomenon, nonlinear transmission experiments in CH_3CN solutions in a 2-mm cuvette were carried out at 532 nm using 4.1-ns laser pulses. For easy comparison between **Ir-1** and **Ir-2**, the linear transmission of each sample solution was adjusted to 80% in the 2-mm cuvette at 532 nm. The transmittance vs. incident energy curves for **Ir-1** and **Ir-2** are presented in Fig. 4. Upon increasing the incident energy, the transmittance of **Ir-1** and **Ir-2** decreases pronouncedly, indicating the occurrence of RSA. The RSA strengths of these two complexes are quite similar to each other, with **Ir-1** exhibiting a slightly stronger RSA than **Ir-2**, suggesting that extending the π -conjugation of the bridging ligand slightly enhances the RSA of this dinuclear Ir(III) complex. Moreover, the RSA of **Ir-1** and **Ir-2** resembles that of the corresponding mononuclear Ir(III) complex bearing fluorenyl-substituted quqo ($\text{N}^{\wedge}\text{N}$) and piq ($\text{C}^{\wedge}\text{N}$) ligands,⁴⁶ reflecting that these dinuclear complexes retain the similar triplet excited-state properties to those of their mononuclear counterparts. These results also manifest the feasibility of dinuclear Ir(III) complexes for optical limiting.

It is known that the key parameter determining the strength of RSA is the ratio of the excited-state absorption cross section (σ_{ex}) vs the ground-state absorption cross section (σ_0) at the interested wavelength, i.e. 532 nm. The σ_0 values can be deduced from the molar extinction coefficients of the ground-state absorption, while the σ_{ex} values can be estimated from the ΔOD values at 532 nm and the TA band maximum, and the $\epsilon_{\text{T}_1-\text{T}_n}$ value at the TA band maximum according to the method previously reported by our group.⁶⁹ The resultant values presented in Table 4 demonstrate that extending the π -conjugation of the bridging ligand in **Ir-1** increases the σ_0 value at 532 nm slightly; however, such a structural variation almost doubles its σ_{ex} value at 532 nm compared to those of **Ir-2**. Consequently, **Ir-1** possesses a larger $\sigma_{\text{ex}}/\sigma_0$ ratio than **Ir-2** does, leading to a stronger RSA at 532 nm.

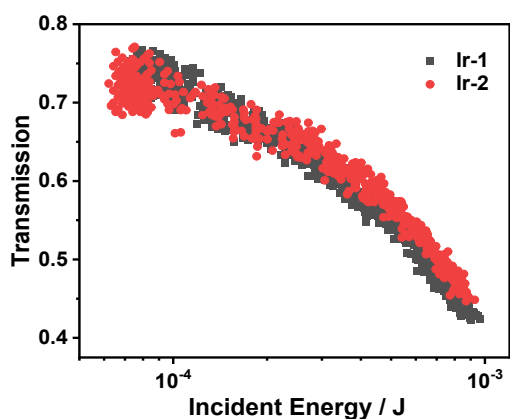


Fig. 4 Nonlinear transmission curves of Ir-1 and Ir-2 in CH₃CN in a 2-mm cuvette for 4.1-ns laser pulses at 532 nm. The linear transmission was adjusted to 80% at 532 nm for both sample solutions. The radius of the beam waist at the focal plane was ~ 96 μ m.

Table 4 Ground-state (σ_0) and excited-state (σ_{ex}) absorption cross sections of complexes Ir-1–Ir-2 in CH₃CN.

	Ir-1	Ir-2
$\sigma_0/10^{-17}$ cm ²	1.69	1.57
$\sigma_{ex}/10^{-17}$ cm ²	20	11.1
σ_{ex}/σ_0	12	7

Conclusions

Our systematic photophysical studies on the two dinuclear Ir(III) complexes bearing fluorenyl-tethered quqo ligand reveal that these complexes exhibit intense ligand-localized $^1\text{ILCT}/^1\pi,\pi^*$ transitions at ca. 330 nm and 400–500 nm, respectively, and $^1,^3\text{MLCT}/^1,^3\text{LLCT}$ transitions at >500 nm. Both complexes emit dual phosphorescence at ca. 590 nm and 710 nm, which are emanated from the $^3\text{ILCT}/^3\pi,\pi^*$ and $^3\text{MLCT}/^3\text{LLCT}$ states, respectively. The low energy $^3\text{MLCT}/^3\text{LLCT}$ state is also responsible for the moderately strong transient absorption at 490–800 nm. It appears that electron density distribution of the T₁ state is mainly localized on one of the (quqo)Ir(piq)₂⁺ units, indicating no communication between the two (quqo)Ir(piq)₂⁺ units. Extending the π -conjugation of the bridging ligand caused a slight red-shift of the $^1\text{ILCT}/^1\pi,\pi^*$ absorption bands and the triplet transient absorbing band at 490–600 nm. The stronger triplet excited-state absorption in the visible spectral region renders these complexes moderately strong RSA at 532 nm for ns laser pulses, which demonstrates the feasibility of the dinuclear complexes as a reverse saturable absorber and is the first time that such a phenomenon is reported for dinuclear Ir(III) complexes. With further structural modifications of the bridging ligand and/or C^N ligand to shift the T₁ state to the bridging ligand localized $^3\pi,\pi^*$ state, the T₁ state lifetime of this type of dinuclear complexes could be prolonged and the RSA be improved for potential optical limiting applications. After the photophysics and RSA of the dinuclear complexes are optimized, the complexes with the best RSA performance in solutions will be doped into solid matrix for practice optical limiting tests.

Conflicts of interest

There are no conflicts to declare.

Acknowledgements

W. Sun and S. Kilina thank the National Science Foundation (DMR-1411086) for support. S. Kilina also acknowledges the Center for Computationally Assisted Science and Technology (CCAST) at North Dakota State University for computer access and administrative support.

References

- 1 I. M. Dixon, J.–P. Collin, J.–P. Sauvage, L. Flamigni, S. Encinas and F. Barigelletti, *Chem. Soc. Rev.*, 2000, **29**, 385–391.
- 2 S. Lamansky, P. Djurovich, D. Murphy, F. Abdel-Razzaq, R. Kwong, I. Tsyba, M. Bortz, B. Mui, R. Bau and M. E. Thompson, *Inorg. Chem.*, 2001, **40**, 1704–1711.
- 3 J. I. Goldsmith, W. R. Hudson, M. S. Lowry, T. H. Anderson and S. Bernhard, *J. Am. Chem. Soc.*, 2005, **127**, 7502–7510.
- 4 E. Holder, B. M. W. Langeveld and U. S. Schubert, *Adv. Mater.*, 2005, **17**, 1109–1121.
- 5 H.–T. Mao, G.–F. Mao, G.–G. Shan, X.–L. Wang and Z.–M. Su, *Coord. Chem. Rev.*, 2020, **413**, 213283.
- 6 H. Xu; R. Chen, Q. Sun, W. Lai, Q. Su, W. Huang and X. Liu, *Chem. Soc. Rev.*, 2014, **43**, 3259–3302.
- 7 T.–Y. Li, J. Wu, Z.–G. Wu, Y.–X. Zheng, J.–L. Zuo and Y. Pan, *Coord. Chem. Rev.*, 2018, **374**, 55–92.
- 8 M. Mydlak, C. Bizzarri, D. Hartmann, W. Sarfert, G. Schmid and L. De Cola, *Adv. Funct. Mater.*, 2010, **20**, 1812–1820.
- 9 J. Sun, F. Zhong, X. Yi and J. Zhao, *Inorg. Chem.*, 2013, **52**, 6299–6310.
- 10 Y. Li, N. Dandu, R. Liu, Z. Li, S. Kilina and W. Sun, *J. Phys. Chem. C*, 2014, **118**, 6372–6384.
- 11 W. Sun, C. Pei, T. Lu, P. Cui, Z. Li, C. McCleese, Y. Fang, S. Kilina, Y. Song and C. Burda, *J. Mater. Chem. C*, 2016, **4**, 5059–5072.
- 12 H. Huo, X. Shen, C. Wang, L. Zhang, P. Rose, L.–A. Chen, K. Harms, M. Marsch, G. Hilt and E. Meggers, *Nature*, 2014, **515**, 100–103.
- 13 X. Lang, J. Zhao and X. Chen, *Chem. Soc. Rev.*, 2016, **45**, 3026–3038.
- 14 Y. Chen, R. Guan, C. Zhang, J. Huang, L. Ji and H. Chao, *Coord. Chem. Rev.*, 2016, **310**, 16–40.
- 15 L. Wang, H. Yin, P. Cui, M. Hetu, C. Wang, S. Monro, R. D. Schaller, C. G. Cameron, B. Liu, S. Kilina, S. A. McFarland and W. Sun, *Dalton. Trans.*, 2017, **46**, 8091–8103.
- 16 L. K. McKenzie, I. V. Sazanovich, E. Baggaley, M. Bonneau, V. Guerschais, J. A. G. Williams, J. A. Weinstein and H. E. Bryant, *Chem. Eur. J.*, 2017, **23**, 234–238.
- 17 F. Neve, M. La Deda, A. Crispini, A. Bellusci, F. Puntoriero and S. Campagna, *Organometallics*, 2004, **23**, 5856–5863.
- 18 S. Ladouceur, D. Fortin and E. Zysman-Colman, *Inorg. Chem.*, 2010, **49**, 5625–5641.

- 19 X. Zhu, L. Lystrom, S. Kilina and W. Sun, *Inorg. Chem.*, 2016, **55**, 11908–11919.
- 20 R.-D. Costa, F. Monti, G. Accorsi, A. Barbieri, H.-J. Bolink, E. Orti and N. Armaroli, *Inorg. Chem.*, 2011, **50**, 7229–7238.
- 21 X. Zeng, M. Tavasli, I. Perepichka, A. Batsanov, M. Bryce, C. Chiang, C. Rothe and A. P. Monkman, *Chem. Eur. J.*, 2008, **14**, 933–943.
- 22 Q. Zhao, S. Liu, M. Shi, C. Wang, M. Yu, L. Li, F. Li, T. Yi and C. Huang, *Inorg. Chem.*, 2006, **45**, 6152–6160.
- 23 K.-Y. Kim, R. T. Farley and K. S. Schanze, *J. Phys. Chem. B*, 2006, **110**, 17302–17304.
- 24 L. Wang, P. Cui, S. Kilina and W. Sun, *J. Phys. Chem. C*, 2017, **121**, 5719–5730.
- 25 B. Liu, L. Lystrom, S. Kilina and W. Sun, *Inorg. Chem.*, 2019, **58**, 476–488.
- 26 Z. Li, P. Cui, C. Wang, S. Kilina and W. Sun, *J. Phys. Chem. C*, 2014, **118**, 28764–28775.
- 27 C. Wang, L. Lystrom, H. Yin, M. Hetu, S. Kilina, S. A. McFarland and W. Sun, *Dalton Trans.*, 2016, **45**, 16366–16378.
- 28 C. Pei, P. Cui, C. McCleese, S. Kilina, C. Burda and W. Sun, *Dalton Trans.*, 2015, **44**, 2176–2190.
- 29 B. Liu, L. Lystrom, S. L. Brown, E. K. Hobbie, S. Kilina and W. Sun, *Inorg. Chem.*, 2019, **58**, 5483–5493.
- 30 G. Li, D. Zhu, X. Wang, Z. Su and M. R. Bryce, *Chem. Soc. Rev.*, 2020, **49**, 765–838.
- 31 J.-L. Liao, P. Rajakannu, P. Gnanasekaran, S.-R. Tsai, C.-H. Lin, S.-H. Liu, C.-H. Chang, G.-H. Lee, P.-T. Chou, Z.-N. Chen and Y. Chi, *Adv. Opt. Mater.*, 2018, **6**, 1800083.
- 32 G. Li, W. Guan, S. Du, D. Zhu, G. Shan, X. Zhu, L. Yan, Z. Su, M. R. Bryce and A. P. Monkman, *Chem. Commun.*, 2015, **51**, 16924–16927.
- 33 Y. Cui, L.-L. Wen, G.-G. Shan, H.-Z. Sun, H.-T. Mao, M. Zhang and Z.-M. Su, *Actuators B*, 2017, **244**, 314–322.
- 34 Y. Chen, W. Xu, J. Zuo, L. Ji and H. Chao, *J. Mater. Chem. B*, 2015, **3**, 3306–3314.
- 35 X. Zhu, B. Liu, P. Cui, S. Kilina and W. Sun, *Inorg. Chem.*, 2020, **59**, 17096–17108.
- 36 G. Li, D. G. Congrave, D. Zhu, Z. Su and M. R. Bryce, *Polyhedron*, 2018, **140**, 146–157.
- 37 W.-J. Xu, S.-J. Liu, X. Zhao, N. Zhao, Z.-Q. Liu, H. Xu, H. Liang, Q. Zhao, X.-Q. Yu and W. Huang, *Chem. Eur. J.*, 2013, **19**, 621–629.
- 38 J. Wang, Y. Lu, N. McGoldrick, C. Zhang, W. Yang, J. Zhao and S. M. Draper, *J. Mater. Chem. C*, 2016, **4**, 6131–6139.
- 39 E. A. Plummer, J. W. Hofstraat and L. De Cola, *Dalton Trans.*, 2003, 2080–2084.
- 40 G. Nasr, A. Guerlin, F. Dumur, L. Beouch, E. Dumas, G. Clavier, F. Miomandre, F. Goubard, D. Gigmes, D. Bertin, G. Wantz and C. R. Mayer, *Chem. Commun.*, 2011, **47**, 10698–10700.
- 41 L. Donato, C. E. McCusker, F. N. Castellano and E. Zysman-Colman, *Inorg. Chem.*, 2013, **52**, 8495–8504.
- 42 T. B. Gao, J.-J. Zhang, J. Wen, X.-X. Yang, H.-B. Ma, D.-K. Cao and D. Jiang, *Anal. Chem.*, 2020, **92**, 1268–1275.
- 43 C. Lu, W. Xu, H. Shah, B. Liu, W. Xu, L. Sun, S. Y. Qian and W. Sun, *ACS Appl. Bio Mater.*, 2020, **3**, 6865–6875.
- 44 S. Yoon and T. S. Teets, *Chem. Commun.*, 2021, **57**, 1975–1988.
- 45 B. Liu, L. Lystrom, C. G. Cameron, S. Kilina, S. A. McFarland and W. Sun, *Eur. J. Inorg. Chem.*, 2019, 2208–2215.
- 46 H. Li, S. Liu, L. Lystrom, S. Kilina and W. Sun, *J. Photochem. Photobiol. A*, 2020, **400**, 112609.
- 47 Z. Ji, S. Li, Y. Li and W. Sun, *Inorg. Chem.*, 2010, **49**, 1337–1346.
- 48 J. N. Demas and G. A. Crosby, *J. Phys. Chem.*, 1971, **75**, 991–1024.
- 49 K. Suzuki, A. Kobayashi, S. Kaneko, K. Takehira, T. Yoshihara, H. Ishida, Y. Shiina, S. Oishi and S. Tobita, *Phys. Chem. Chem. Phys.*, 2009, **11**, 9850–9860.
- 50 D. F. Eaton, *Pure Appl. Chem.*, 1988, **60**, 1107–1114.
- 51 I. Carmichael and G. L. Hug, *J. Phys. Chem. Ref. Data*, 1986, **15**, 1–250.
- 52 C. V. Kumar, L. Kumar, P. K. Das, *J. Chem. Soc., Faraday Trans. 2*, 1984, **80**, 783–793.
- 53 P. A. Firey, W. E. Firey, J. R. Firey, M. E. Kenney and M. A. Rodgers, *J. Am. Chem. Soc.*, 1988, **110**, 7626–7630.
- 54 M. J. Frisch, G. W. Trucks, H. B. Schlegel, G. E. Scuseria, M. A. Robb, J. R. Cheeseman, G. Scalmani, V. Barone, G. A. Petersson, H. Nakatsuji, X. Li, M. Caricato, A. Marenich, J. Bloino, B. G. Janesko, R. Gomperts, B. Mennucci, H. P. Hratchian, J. V. Ortiz, A. F. Izmaylov, J. L. Sonnenberg, D. Williams-Young, F. Ding, F. Lipparini, F. Egidi, J. Goings, B. Peng, A. Petrone, T. Henderson, D. Ranasinghe, V. G. Zakrzewski, J. Gao, N. Rega, G. Zheng, W. Liang, M. Hada, M. Ehara, K. Toyota, R. Fukuda, J. Hasegawa, M. Ishida, T. Nakajima, Y. Honda, O. Kitao, H. Nakai, T. Vreven, K. Throssell, J. A. Montgomery, Jr., J. E. Peralta, F. Ogliaro, M. Bearpark, J. J. Heyd, E. Brothers, K. N. Kudin, V. N. Staroverov, T. Keith, R. Kobayashi, J. Normand, K. Raghavachari, A. Rendell, J. C. Burant, S. S. Iyengar, J. Tomasi, M. Cossi, J. M. Millam, M. Klene, C. Adamo, R. Cammi, J. W. Ochterski, R. L. Martin, K. Morokuma, O. Farkas, J. B. Foresman, and D. J. Fox, Gaussian09, Revision D.01, Gaussian, Inc., Wallingford CT.
- 55 J. E. Peralta and G. E. Scuseria, *J. Chem. Phys.*, 2004, **120**, 5875–5881.
- 56 A. Wolf, M. Reiher and B. A. Hess, *J. Chem. Phys.*, 2002, **117**, 9215–9226.
- 57 M. E. Casida, *Recent Advances in Density Functional Methods (Part I)*, 1995, 155–192.
- 58 R. Bauernschmitt and R. Ahlrichs, *Chem. Phys. Lett.*, 1996, **256**, 454–464.
- 59 E. R. Davidson, *J. Comput. Phys.*, 1975, **17**, 87–94.
- 60 J. P. Perdew, K. Burke and M. Ernzerhof, *Phys. Rev. Lett.*, 1996, **77**, 3865–3868.
- 61 M. Cossi, N. Rega, G. Scalmani and V. Barone, *J. Comput. Chem.*, 2003, **24**, 669–681.
- 62 R. Cammi, S. Corni, B. Mennucci and J. Tomasi, *J. Chem. Phys.*, 2005, **122**, 104513.
- 63 R. L. Martin, *J. Chem. Phys.*, 2003, **118**, 4775–4777.
- 64 G. Zhurko and D. Zhurko, *ChemCraft*, 2009, version 1.6, Build.
- 65 S. Wu, J. Ling, S. Lai, M. Huang, C. Cheng, and I. Chen, *J. Phys. Chem. A*, 2010, **114**, 10339–10344.

Journal Name

ARTICLE

66 C. Li, L. Zhang, R. Wang, Y. Song and Y. Wang, *J. Opt. Soc. Am. B*, 1994, **11**, 1356-1360.

67 A. Penzkofer, *Appl. Phys. B*, 1988, **46**, 43-46.

68 Y. B. Band, D. Harter and R. Bavli, *Chem. Phys. Lett.*, 1986, **126**, 280-284.

69 Y. Li, R. Liu, E. Badaeva, S. Kilina and W. Sun, *J. Phys. Chem. C*, 2013, **117**, 5908-5918.